IOP Publishing Plasma Physics and Controlled Fusion
Plasma Phys. Control. Fusion **62** (2020) 042001 (7pp) https://doi.org/10.1088/1361-6587/ab759c

Note

Spectral treatment of gyrokinetic profile curvature

J Candy[1], **E A Belli and G Staebler**

General Atomics, PO Box 85608, San Diego, CA 92186-5608, United States of America

E-mail: candy@fusion.gat.com

Received 20 November 2019, revised 24 January 2020
Accepted for publication 12 February 2020
Published 26 February 2020

Abstract

Using a novel wavenumber-advection algorithm, we show that profile curvature (shear in the profile gradient) can be implemented with spectral accuracy in gyrokinetic turbulence simulations. This approach enables a global simulation capability with the relatively low cost and high accuracy of local simulations. Using this new algorithm, we show that for a well-studied tokamak core test case, the effect of temperature-gradient curvature is below the threshold of detectability for experimentally-relevant values of curvature.

Keywords: gyrokinetic, turbulence, shear, global, spectral

(Some figures may appear in colour only in the online journal)

1. Introduction and background

1.1. Conceptual motivation

Radial variation, or shear, in the equilibrium $\mathbf{E} \times \mathbf{B}$ velocity is well-known to have a profound stabilizing effect on drift-wave turbulence. The importance of including this global shearing effect in nonlinear simulations of tokamak turbulence has long been recognized [1–5]. Relatedly, the conceptual possibility of transport reduction through *profile curvature* [5, 6] was considered by Waltz and Garbet more than 20 years ago. These key global effects, not directly treatable by a flux-tube code[2], provided the motivation for development of radially-nonperiodic global gyrokinetic codes. However, the capability to treat $\mathbf{E} \times \mathbf{B}$ shear is possible within the flux-tube framework. To wit, the *wavenumber-remapping* method [7, 8] was used successfully to implement $\mathbf{E} \times \mathbf{B}$ shear by exploiting the property that toroidal Fourier harmonics return to radial periodicity at integer multiples of a critical time [7, 9]. For a fixed radial domain size, however, the discretization error is fixed and cannot be reduced by resolving higher wavenumbers. Moreover, the time-dependence of the solution is mildly discontinuous. More importantly, the wavenumber-shift method is applicable only to $\mathbf{E} \times \mathbf{B}$ shear but not to profile curvature—because profile curvature does not cause a simple Doppler shift of the time derivative. For these reasons, a new approach to treat $\mathbf{E} \times \mathbf{B}$ shear by continuous advection of radial wavenumbers was developed [10]. This *wavenumber-advection* approach was shown to produce energy and momentum fluxes that agree well with global simulation results. The new approach simultaneously eliminates (1) certain negative aspects of the wavenumber-shift algorithm and (2) ad hoc radial boundary conditions required by global simulations. In this work, we outline a new approach to the calculation of global *profile curvature* (shear in the temperature and density gradients) by constructing a suitable generalization of the wavenumber advection method. Using this approach, we show that profile curvature can be implemented with spectral accuracy in gyrokinetic turbulence simulations. This enables one to carry out global simulations with the relatively low cost and high accuracy of local simulations. Preliminary nonlinear simulation results for a well-studied test case demonstrate that the effect of temperature-gradient curvature (shear in the temperature gradient) is below the threshold of detectability for experimentally-relevant values of the curvature in the core of tokamaks.

[1] Author to whom any correspondence should be addressed.
[2] A flux-tube code assumes a doubly-periodic 2D domain in the radial and binormal directions.

1.2. Profile curvature

Consider the profiles of density and temperature gradient

$$\kappa_a^{\mathrm{N}} \doteq -\frac{a}{n_a}\frac{dn_a}{dr} = \frac{a}{L_{na}}, \tag{1}$$

$$\kappa_a^{\mathrm{T}} \doteq -\frac{a}{T_a}\frac{dT_a}{dr} = \frac{a}{L_{Ta}}. \tag{2}$$

Above, r is the midplane minor radius, a is the minor radius of the LCFS, and the subscript a denotes a species index. Linear growth rates and associated nonlinear fluxes of heat and particles are well-known to be controlled by the local values of these parameters. Gyrokinetic code benchmark exercises are typically carried out using the Cyclone base case [11] and the GA standard case [4] parameters—characterized by constant values of κ^{N} and κ^{T}. Since the development of the first toroidal gyrokinetic codes in the 1990s, the conceptual possibility of transport reduction through *profile curvature* [5, 12] has been considered. The curvature does not presently have a standard formal definition, so in this work we define the density and temperature curvature as

$$s_a^{\mathrm{N}} \doteq -\frac{a}{n_a}\frac{d^2n_a}{dr^2}\rho_s, \tag{3}$$

$$s_a^{\mathrm{T}} \doteq -\frac{a}{T_a}\frac{d^2T_a}{dr^2}\rho_s. \tag{4}$$

Here, ρ_s is the *effective ion-sound gyroradius*

$$\rho_s \doteq \frac{c_s}{eB_{\mathrm{unit}}/(m_{\mathrm{D}}c)}. \tag{5}$$

The explicit appearance of ρ_s in equations (3) and (4) is required to maintain the proper analytic scaling of the curvature, which should vanish in the limit $\rho_s/a \doteq \rho_* \to 0$. In the definition of ρ_s, B_{unit} is the *effective magnetic field* [13, 14]. This is independent of poloidal angle, and defined with reference to a global equilibrium through the relation

$$B_{\mathrm{unit}}(r) = \frac{q}{r}\psi', \tag{6}$$

where $\psi' \doteq \partial\psi/\partial r$. At mid-radius in the DIII-D tokamak, typical curvatures are on the order of $s_a^{\mathrm{N}} \sim s_a^{\mathrm{T}} \sim 0.01$ when $\kappa_a^{\mathrm{N}} \sim \kappa_a^{\mathrm{T}} \sim 1.0$. In a gyrokinetic simulation with $L = 100\rho_s$, for example, the ion density gradient scale length would vary by an amount $\Delta(a/L_{ni}) = 1.0$ over the simulation domain when $s_i^{\mathrm{N}} = 0.01$. Like the rotation profile, the equilibrium density and temperature are free profiles in the gyrokinetic equation and determined by the respective transport equations at $\mathcal{O}(\rho_*^2)$.

1.3. Consistency with the drift ordering

The profile curvature terms associated with equations (3) and (4) are formally one order smaller in ρ_* than those required by the drift ordering [15, 16]. Evidently, there are myriad other formally negligible terms that could also be added to the gyrokinetic equation. Thus, if profile curvature is measurable in a gyrokinetic simulation, then other small corrections might also be measurable. For this reason we must explain our motivation. Interest in profile curvature dates back more than two decades, when it was speculated that the shear in the diamagnetic frequency (proportional to s_a^{N} and s_a^{T}) might provide a stabilization comparable to the shear in the $\mathbf{E}\times\mathbf{B}$ velocity (γ_E) [5]. Prior simulations attempting to quantify this have been carried out [6, 12], but the effects are small and difficult to measure accurately. Thus, in treating curvature spectrally, we can make a higher-precision estimate of curvature-driven stabilization than in previous work. If curvature-driven stabilization is significant, it would be an indication that the gyrokinetic ordering itself is in jeopardy. Alas, for the test cases considered in this paper, no significant stabilization is observed. A similar null result was found, some time ago, for the (higher-order) parallel nonlinearity [17].

1.4. Spectral treatment of nonperiodic phenomena

To avoid later confusion, we will clarify some important nomenclature. In this work, a *local* simulation [9, 18] is one in which the coefficients of the gyrokinetic equation are constant and solutions doubly periodic in the radial and binormal directions. An oft-used synonym for local is *flux-tube*. Local simulations normally use a Fourier representation of fluctuations, but this is not necessary. In principle, local simulations can use mesh-based finite-differences (GYRO local simulations are one example). In contrast to a local simulation is a *global* simulation [19–21]. In principle, *global* could refer to any simulation that is not local; for example, a simulation with constant coefficients (no profile variation) and Dirichlet (nonperiodic) boundary conditions. Of course this is not standard usage of the term. More commonly, a global simulation is nonperiodic and retains some coefficient variation in the radial direction. With respect to the simulation technique, *spectral* implies a manifestly periodic 2D Fourier mode representation in the radial and binormal directions. Spectral gyrokinetic solvers achieve high computational efficiency and accuracy [22] by working directly in wavenumber space thereby reducing the gyroaverage to multiplication by a Bessel function. Because of the periodicity of fluctuations, spurious behaviour including boundaries instabilities [21] and profile flattening [6, 23] are eliminated. In addition, simulations that require simultaneous resolution of electron-scale and ion-scale turbulence [24, 25] benefit greatly from spectral algorithms. A technically precise description of the contrast between flux-tube and global simulations, and a prescription for treating global terms in a flux-tube framework, has also been given by Parra [26] and we refer the reader thereto for more information.

Historically, because a spectral basis implies periodicity of fluctuations in the radial and binormal directions, researchers were mostly resigned to the opinion that turbulence stabilization due to profile curvature, along with other mesoscale transport phenomena, are amenable only to traditional nonperiodic global simulation. This reasoning directly motivated the development of GYRO [21] in 1999. Over the years, comparisons between local and global simulation have seen some confluence as (1) profile relaxation effects generated in global simulations have been eliminated, (2) methods

to treat $\mathbf{E}\times\mathbf{B}$ shear with reasonable fidelity were developed for flux-tube codes [7]. For example, very recent simulations of ASDEX [27] and TCV [28] show that local-global differences are small or negligible when profile relaxation is properly mitigated. These shrinking differences between local and global simulations give rise to a catch-22 in which the lower fidelity of global codes with respect to $\mathcal{O}(1)$ local physics makes them less able to reliably compute the small $\mathcal{O}(\rho_*)$ corrections they were designed for[3]. This sobering realization was a key motivation for the development of CGYRO [29]. The CGYRO strategy is to optimize the performance and accuracy of the dominant, leading-order gyrokinetic dynamics, and then seek new approaches to deal with highly subdominant mesoscale phenomena.

With the development of the wavenumber advection method, a new possibility for high accuracy *global-spectral* simulation emerges in which coefficients of the gyrokinetic equation may retain physical radial variation over a subdomain of a larger periodic computational domain. More generally, spectral representation of nonperiodic functions as a research topic has received significant attention [30–32] and is closely connected to Chebyshev approximation.

2. Theoretical formulation

2.1. Spectral representation of fluctuations

In the recursive formulation of nonlinear electromagnetic gyrokinetic theory [16, 33], fluctuations are represented in eikonal (ballooning) form as

$$h_a(\mathbf{R}) = \sum_{\mathbf{k}_\perp} e^{iS_{\mathbf{k}}(\mathbf{R})} h_{a,\mathbf{k}_\perp}, \tag{7}$$

where $\mathbf{k}_\perp \doteq \nabla_\perp S_{\mathbf{k}}$ is the perpendicular wavenumber, $\mathbf{R}$ is the location of a gyrocenter, and a is the species index. In this paper, we use the non-orthogonal field-aligned coordinate system (ψ, θ, α) together with the Clebsch representation for the magnetic field [34], $\mathbf{B} = \nabla\alpha \times \nabla\psi$. Here, $\alpha \doteq \varphi + \nu(\psi, \theta)$, where φ is the toroidal angle, ψ is the poloidal flux divided by 2π, and θ is the poloidal angle.

A spectral gyrokinetic code expands fluctuations in terms of a *time-independent* eikonal

$$h_a(x, \alpha, t) = f_{0a} \sum_{n=-N}^{N} \sum_{p=-M}^{M} e^{ipx} e^{-in\alpha}\, \widetilde{h}_a(n, p, t), \tag{8}$$

where $S_{\mathbf{k}} = px - n\alpha$. In these expressions, f_{0a} is the zeroth-order equilibrium Maxwellian distribution for species a. The Fourier representation in equation (8) is clarified further in section 3 of [29]. In equation (8), we have defined an angular radial variable $x = 2\pi(r - r_0)/L \in [0, 2\pi)$, where L is the radial width of the simulation domain. As in equation (15) of [10], the spectral gyrokinetic equation is written symbolically as

$$\left.\frac{\partial \widetilde{h}_a}{\partial t}\right|_{\text{unsheared}} = \mathcal{G}(n, p, \widetilde{h}_a). \tag{9}$$

The expression above reflects the CGYRO formulation as written in equation (27) of [35] for the case of sonic rotation, or in equation (57) of [29] for the simpler case of diamagnetic toroidal rotation. We can make contact with [29, 35] by writing

$$\left(\frac{a}{c_s}\right)\mathcal{G}(n, p, \widetilde{h}_a) \doteq i(\Omega_\theta + \Omega_\xi + \Omega_{\rm d})\widetilde{H}_a + i\Omega_*\widetilde{\Psi}_a - \frac{2\pi a}{L}\frac{q\rho_s}{r}\,\widetilde{h}_a * \widetilde{\Psi}_a + \frac{a}{c_s}\textstyle\sum_b C^L_{ab}(\widetilde{H}_a, \widetilde{H}_b), \tag{10}$$

where $c_s = \sqrt{T_e/m_{\rm D}}$ is the deuteron sound speed, T_e is the electron temperature, and $m_{\rm D}$ is the deuteron mass. General, explicit forms for $\widetilde{H}_a$, Ω_θ, Ω_ξ, $\Omega_{\rm d}$, Ω_*, $\widetilde{\Psi}_a$, C^L_{ab} and $*$ (a generalized convolution) are given in [35].

2.2. Wavenumber advection

$\mathbf{E}\times\mathbf{B}$ shear and profile curvature can now be treated using the same spectral representation of fluctuations defined in equation (8). We do this by employing a *periodization* of the nonperiodic function x in terms of a spectral shearing operator X. The details of this periodization, including discussion of naive and inaccurate forms of X, are given in [10]. Using X we can write a periodic spectral GK equation including the effect of $\mathbf{E}\times\mathbf{B}$ shear and density/temperature curvature

$$\begin{aligned}\frac{a}{c_s}\frac{\partial \widetilde{h}_a}{\partial t} = {} & \mathcal{G}(n, p, \widetilde{h}_a) \\ & - i\,\frac{k_\theta L}{2\pi}\,\frac{a\gamma_E}{c_s}\,X\widetilde{h}_a && (\mathbf{E}\times\mathbf{B}\text{ shear}) \\ & - i\,\frac{k_\theta L}{2\pi}\,s_a^{\rm N}\,X\widetilde{\Psi}_a && (n\quad\text{curvature}) \\ & - i\,\frac{k_\theta L}{2\pi}\,s_a^{\rm T}\,(u_a^2 - 3/2)X\widetilde{\Psi}_a && (T\quad\text{curvature}).\end{aligned} \tag{11}$$

Here, $u_a \doteq v/(\sqrt{2}\,v_{ta})$ with v_{ta} the thermal velocity of species a. X is an operator on the space of discrete functions f given by

$$-iXf(n, p) = \sum_k a_k[f(n, p + k) - f(n, p - k)]. \tag{12}$$

The decorrelation rate in the presence of sheared $\mathbf{E}\times\mathbf{B}$ flow is given by the *Waltz shearing rate* [1]

$$\gamma_E \doteq -\frac{r}{q}\frac{d\omega_0}{dr}. \tag{13}$$

In [10], a two-term expansion was recommended, with $a_1 = 2/\pi$ and $a_3 = -2/(9\pi)$. Retaining only 2 terms in the series ensures that the shearing is driven by only the two longest (equilibrium-scale) waves in the system. Physically, the wavenumber advection method represents two simulations: one with positive shearing connected smoothly to one with negative shearing. It is important to note that, since the

[3] In particular, error control in connection with sources, boundary conditions, electron dynamics and electromagnetic modes is more challenging globally.

shearing represents only a *small perturbation* to the unsheared system, the unphysical Dirichlet-type boundary conditions normally used in global simulations are replaced by elegant inflow/outflow boundaries. In the case of $\mathbf{E} \times \mathbf{B}$ shear, a *spectral shift* in the fluctuation spectrum is induced [36], and a model of this shift is the basis for implementation in the TGLF [37] transport model.

2.3. Time-delay kinetic source

To complete the formulation we define a source in terms of a time-delay operator acting only on the longest-wavelength zonal mode $\widetilde{h}_a(0,\,1)$:

$$\frac{\partial \widetilde{h}_a(0,\,1)}{\partial t} = -\nu_s \langle \widetilde{h}_a(0,\,1)\rangle_\tau, \tag{14}$$

where

$$\langle f\rangle_\tau(t) \doteq \frac{\int_0^t dt' \exp(t'/\tau) f(t')}{\int_0^t dt' \exp(t'/\tau)}. \tag{15}$$

This source, to be added to equation (11), prohibits relaxation of all velocity-space moments of the distribution, including particles, momentum, and energy. It is now well-understood that sources of particles, momentum and energy must be included to maintain density, rotation and temperature profiles [26]. Because the source in equation (14) acts only on the zonal ($n = 0$) component, there is no unphysical effect on linear growth rates via finite-k_y dissipation [38]. For the simulations reported herein we have selected $(c_s/a)\tau = 50.0$, which is the same value used in the original GYRO time-delay source (circa 2002) [6]. The source rate is taken to be proportional to the shearing rate: for example, $(a/c_s)\nu_s = 10 s_{\rm D}^{\rm T}$. To obtain the conjugate mode $\widetilde{h}_a(0,\,-1)$ we simply set $\widetilde{h}_a(0,\,-1) = \widetilde{h}_a(0,\,1)^*$. Finally, we remark that the equilibrium mode $\widetilde{h}_a(0,\,0)$ is undetermined by gyrokinetic theory[4] and thus is absent from the simulation.

3. Performance of the new approach

To assess the performance of the new approach we carried out numerous nonlinear CGYRO simulations—both with adiabatic and kinetic electrons—based on the General Atomics (GA) standard case parameters [4]: $R_0/a = 3$, $r/a = 0.5$, $q = 2$, $s = 1$, $T_i = T_e$. The geometry is a Grad–Shafranov unshifted circular equilibrium with metric coefficients generated using the Miller local formalism [40, 41]. All simulations retained 16 discrete complex toroidal modes

$$k_y \rho_s = 0.0,\, 0.05,\, 0.1,\, \ldots,\, 0.75, \tag{16}$$

with $k_y = nq/r$. This binormal resolution corresponds to $N = 15$ in equation (8), although modes with $n < 0$ do not need to be simulated because reality of the physical fields implies $\widetilde{h}_a(-n,\,-p) = \widetilde{h}_a^*(n,\,p)$. In the radial direction we used 180 radial wavenumbers ($M = 90$) thereby resolving $0 \leqslant k_x \rho_s \leqslant 2.80$. The radial and binormal domain sizes were taken to be $L = 200\ \rho_s$ and $L_y = 126\ \rho_s$, respectively. Density gradients were fixed in all cases: $\kappa_{\rm D}^{\rm N} = \kappa_e^{\rm N} = 1$.

[4] The poloidal dependence of the (0, 0) mode is effectively determined by neoclassical theory [39] whereas its flux-surface average is determined by the transport equations [16].

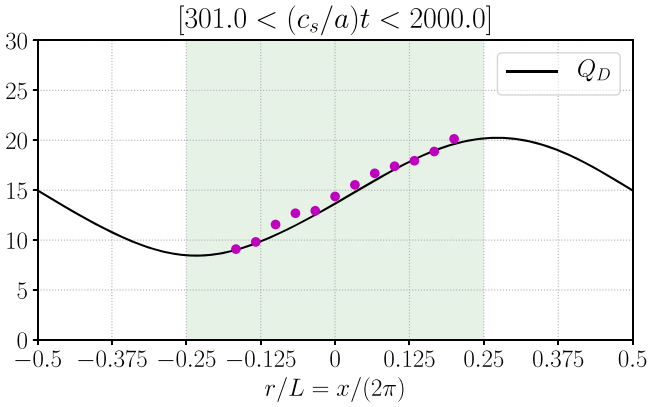

Figure 1. Global flux profile (solid curve) for GA standard case (adiabatic electrons) with $s_{\rm D}^{\rm T} = 0.015$, compared with equivalent local simulations (magenta dots). Deviation from the local result is less than the statistical uncertainty of the time-averaged fluxes. Green shaded region ($|r/L| \leqslant 0.25$) is the positive (physical) curvature region whereas the unshaded white region ($|r/L| > 0.25$) is the negative (mirror) curvature region.

3.1. Nonlinear global simulations with adiabatic electrons

To begin, we carried out simulations with gyrokinetic deuterium and adiabatic electrons. A small collision frequency $(a/c_s)\nu_{\rm DD} = 0.165 \times 10^{-3}$ was chosen to provide some damping of zonal flows. All runs used fixed timestep $(c_s/a)\Delta t = 0.04$. Because the energy fluxes have a natural gyroBohm scaling, we normalize them to a reference gyroBohm level

$$Q_{\rm GB} = n_e T_e c_s \frac{\rho_s^2}{a^2}. \tag{17}$$

Both global and local simulations were done with CGYRO. The single global CGYRO simulation used density and temperature gradients $\kappa_{\rm D}^{\rm N} = 1$ and $\kappa_{\rm D}^{\rm T} = 3$ respectively, with temperature curvature $s_{\rm D}^{\rm T} = 0.015$ (density curvature was set to zero). The results of this simulation are shown in figure 1, overlaid with results from 12 local simulations for which $\kappa_{\rm D}^{\rm T}$ was varied over the range $2.5 \leqslant \kappa_{\rm D}^{\rm T} \leqslant 3.6$. At this value of $s_{\rm D}^{\rm T}$ we expected to see some evidence of turbulence suppression, but no statistically significant effect was observed. Note that, to achieve very low statistical error, we ran all simulations up to $(c_s/a)t = 2000$, averaging results over the range $300 \leqslant (c_s/a)t \leqslant 2000$. The profile of global energy flux, $Q_{\rm D}$, was obtained by reconstruction using radial wavenumbers $|p| \leqslant 4$ (an arbitrary choice, sufficient to capture the relevant long-wavelength structure).

A second global spectral simulation was carried out with double the shearing rate: $s_{\rm D}^{\rm T} = 0.03$. The results of this more highly-sheared case are shown in figure 2, overlaid with results from the same 12 local simulations. In this case the local simulations are spaced at half the distance they were in

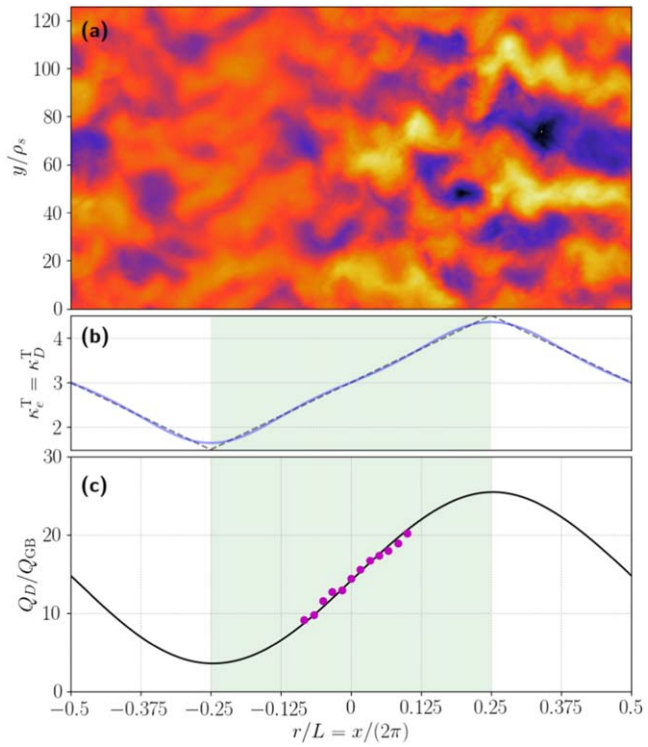

Figure 2. Global spectral simulation (adiabatic electrons) with finite profile curvature, $s_D^T = 0.03$. Frame (a) shows turbulent energy fluctuations with clear increase in intensity at higher gradient. Frame (b) shows profile of effective temperature gradient scale length generated by wavenumber advection scheme. Frame (c) shows the global energy flux profile (solid curve) compared with 12 local simulation (magenta dots). Green shaded region ($|r/L| \leqslant 0.25$) is the positive (physical) curvature region whereas the unshaded white region ($|r/L| > 0.25$) is the negative (mirror) curvature region.

figure 1 because the shearing rate for the global simulation has doubled. In detail, figure 2 shows the turbulent energy fluctuations (frame a) atop the effective density-gradient scale length (frame b) and global energy flux (frame c). As before, the flux profile was obtained by reconstruction using radial wavenumbers $|p| \leqslant 4$. Even at this larger shearing rate, no statistically significant transport reduction is observed. We also clarify that, in figure 2, the green shaded region corresponds to the positive shear domain. In this domain, the gradient scale length varies significantly: from $1.5 \leqslant \kappa_D^T \leqslant 4.5$.

3.2. Nonlinear global simulations with kinetic electrons

To avoid the possibility of misleading results due to the (physically inaccurate) adiabatic electron model, we carried out a second series of simulations with gyrokinetic deuterium and gyrokinetic electrons ($m_D/m_e = 3670$). A much smaller timestep, $(c_s/a)\Delta t = 0.005$, was required. The simulations were electromagnetic with a small value of $\beta_{e,\mathrm{unit}} = 0.05\%$. Collisions were implemented using the Sugama [42, 43] operator with self-consistent collision rates $(a/c_s)\nu_{ee} = 0.1$ and $(a/c_s)\nu_{DD} = 0.165 \times 10^{-3}$. Radial and binormal resolutions were unchanged from the previous section. Six local simulations and one global simulation was carried out. The local simulations spanned the range $2.8 \leqslant \kappa_D^T \leqslant 3.3$.

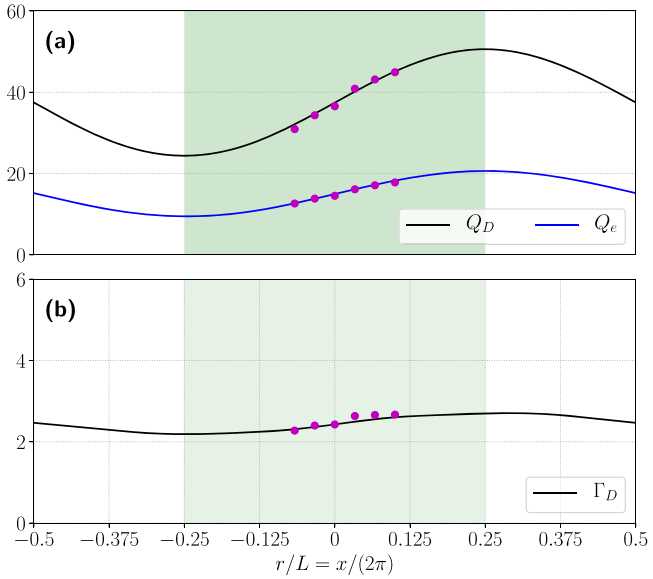

Figure 3. Global flux profiles (solid curves) for GA standard case (gyrokinetic electrons) with $s_D^T = s_e^T = 0.015$, compared with equivalent local simulations (magenta dots). Plot (a) shows ion and electron energy fluxes, and plot (b) shows ion particle flux. Deviation of the global curve from the local results is less than the statistical uncertainty of the time-averaged fluxes. Green shaded region ($|r/L| \leqslant 0.25$) is the positive (physical) curvature region whereas the unshaded white region ($|r/L| > 0.25$) is the negative (mirror) curvature region.

The global simulation had $\kappa_D^T = \kappa_e^T = 3$ and curvatures $s_D^T = s_e^T = 0.015$. The result—shown in figure 3—once again demonstrates surprisingly close agreement between local and global fluxes in all transport channels with no evidence of profile curvature stabilization.

4. Discussion and summary

Using a novel wavenumber-advection algorithm, we have shown that nonlocal profile curvature can be implemented with spectral accuracy in gyrokinetic turbulence simulations. This approach represents an alternative methodology for global gyrokinetic simulation, with the lower cost and higher accuracy of local simulation algorithms. Using this high-accuracy method, we have demonstrated that, for a well-studied test case, the effect of temperature-gradient curvature is below the statistical threshold of detectability for experimentally-relevant values of curvature. Whether this result can be generalized to more realistic experimental parameters is a question for future inquiry.

Acknowledgments

This material is based upon work supported by the U.S. Department of Energy, Office of Science, Office of Fusion Energy Sciences, Theory program, under award DE-FG02-95ER54309, by the Edge Simulation Laboratory project under award DE-FC02-06ER54873 and by the AToM

SciDAC-4 project under award DE-SC0017992. The research used resources of the Oak Ridge Leadership Computing Facility under Contract DE-AC05-00OR22725 via an award of computer time provided by the ALCC program. This report was prepared as an account of work sponsored by an agency of the United States Government. Neither the United States Government nor any agency thereof, nor any of their employees, makes any warranty, express or implied, or assumes any legal liability or responsibility for the accuracy, completeness, or usefulness of any information, apparatus, product, or process disclosed, or represents that its use would not infringe privately owned rights. Reference herein to any specific commercial product, process, or service by trade name, trademark, manufacturer, or otherwise, does not necessarily constitute or imply its endorsement, recommendation, or favoring by the United States Government or any agency thereof. The views and opinions of authors expressed herein do not necessarily state or reflect those of the United States Government or any agency thereof.

ORCID iDs

J Candy https://orcid.org/0000-0003-3884-6485
G Staebler https://orcid.org/0000-0002-1944-1733

References

[1] Waltz R E, Kerbel G R and Milovich J 1994 Toroidal gyro-Landau fluid model turbulence simulations in a nonlinear ballooning mode representation with radial modes *Phys. Plasmas* **1** 2229
[2] Miller R L, Waelbroeck F L, Hassam A B and Waltz R E 1995 Stabilization of ballooning modes with sheared toroidal rotation *Phys. Plasmas* **2** 3676
[3] Dimits A M, Williams T J, Byers J A and Cohen B I 1996 Scalings of ion-temperature-gradient-driven anomalous transport in tokamaks *Phys. Rev. Lett.* **77** 71
[4] Waltz R E, Staebler G M, Dorland W, Hammett G W, Kotschenreuther M and Konings J A 1997 A gyro-landau fluid transport model *Phys. Plasmas* **4** 2482
[5] Waltz R E, Dewar R L and Garbet X 1998 Theory and simulation of rotational shear stabilization of turbulence *Phys. Plasmas* **5** 1784
[6] Waltz R E, Candy J and Rosenbluth M N 2002 Gyrokinetic turbulence simulation of profile shear stabilization and broken gyrobohm scaling *Phys. Plasmas* **9** 1938
[7] Hammett G W *et al* 2006 Implementation of large scale E × B shear flow in the GS2 gyrokinetic turbulence code *Bull. Am. Phys. Soc.* VP1.00136
[8] Casson F J, Peeters A G, Camenen Y, Hornsby W A, Snodin A P, Strinzi D and Szepesi G 2009 Anomalous parallel momentum transport due to E × B flow shear in a tokamak plasma *Phys. Plasmas* **16** 092303
[9] Peeters A G, Camenen Y, Casson F J, Hornsby W A, Snodin A P, Strintzi D and Szepesi G 2009 The nonlinear gyrokinetic flux tube code GKW *Comput. Phys. Commun.* **180** 2650
[10] Candy J and Belli E A 2018 Spectral treatment of gyrokinetic shear flow *J. Comput. Phys.* **356** 448
[11] Dimits A M *et al* 2000 Comparisons and physics basis of tokamak transport models and turbulence simulations *Phys. Plasmas* **7** 969
[12] Waltz R E, Staebler G M and Solomon W M 2011 Gyrokinetic simulation of momentum transport with residual stress from diamagnetic level velocity shears *Phys. Plasmas* **18** 042504
[13] Candy J 2009 A unified method for operator evaluation in local Grad–Shafranov plasma equilibria *Plasma Phys. Control. Fusion* **51** 105009
[14] Waltz R E and Miller R L 1999 Ion temperature gradient turbulence simulations and plasma flux surface shape *Phys. Plasmas* **6** 4265
[15] Sugama H and Horton W 1997a Neoclassical electron and ion transport in toroidally rotating plasmas *Phys. Plasmas* **4** 2215
[16] Sugama H and Horton W 1998 Nonlinear electromagnetic gyrokinetic equation for plasmas with large mean flows *Phys. Plasmas* **5** 2560
[17] Candy J, Waltz R E, Parker S E and Chen Y 2006 Relevance of the parallel nonlinearity in gyrokinetic simulations of tokamak plasmas *Phys. Plasmas* **13** 074501
[18] Dorland W, Jenko F, Kotschenreuther M and Rogers B N 2000 Electron temperature gradient turbulence *Phys. Rev. Lett.* **85** 5579
[19] Parker S E, Kim C and Chen Y 1999 Large-scale gyrokinetic turbulence simulations: effects of profile variation *Phys. Plasmas* **6** 1709
[20] Lin Z, Hahm T S, Lee W W, Tang W M and White R B 2000 Gyrokinetic simulations in general geometry and applications to collisional damping of zonal flows *Phys. Plasmas* **7** 1857
[21] Candy J and Waltz R E 2003 An Eulerian gyrokinetic-Maxwell solver *J. Comput. Phys.* **186** 545
[22] Candy J, Sfiligoi I, Belli E, Hallatschek K, Holland C, Howard N and D`Azevedo E 2019 Multiscale-optimized plasma turbulence simulation on petascale architechtures *Comput. Fluids* **188** 125
[23] Lapillonne X, McMillan B F, Görler T, Brunner S, Dannert T, Jenko F, Merz F and Villard L 2010 Nonlinear quasisteady state benchmark of global gyrokinetic codes *Phys. Plasmas* **17** 112321
[24] Howard N T, White A E, Greenwald M, Reinke M L, Walk J, Holland C, Candy J and Görler T 2013 Investigation of the transport shortfall in alcator c-mod l-mode plasmas *Phys. Plasmas* **20** 032510
[25] Howard N T, Holland C, White A E, Greenwald M and Candy J 2014 Synergistic cross-scale coupling of turbulence in a tokamak plasma *Phys. Plasmas* **21** 112510
[26] Parra F I and Barnes M 2015 Equivalence of two different approaches to global δf gyrokinetic simulations *Plasma Phys. Control. Fusion* **57** 054003
[27] Hornsby W A *et al* 2018 Global gyrokinetic simulations of intrinsic rotation in ASDEX Upgrade Ohmic L-mode plasmas *Nucl. Fusion* **58** 056008
[28] Mariani A, Brunner S, Merlo G and Sauter O 2019 Gyrokinetic analysis of radial dependence and global effects on the zero particle flux condition in a TCV plasma *Plasma Phys. Control. Fusion* **61** 064005
[29] Candy J, Belli E A and Bravenec R V 2016 A high-accuracy Eulerian gyrokinetic solver for collisional plasmas *J. Comput. Phys.* **324** 73
[30] Huybrechs D 2010 On the Fourier extension of nonperiodic functions *SIAM J. Numer. Anal* **47** 4326
[31] Wang J P 1998 Finite spectral method based on non-periodic fourier transform *Comput. Fluids* **27** 639
[32] Boyd J P 2007 Exponentially accurate runge-free approximation of non-periodic functions from samples on an evenly spaced grid *App. Math Lett* **20** 971

[33] Sugama H and Horton W 1997b Transport processes and entropy production in toroidally rotating plasmas with electrostatic turbulence *Phys. Plasmas* **4** 405
[34] Kruskal M D and Kulsrud R M 1958 Equilibrium of a magnetically confined plasma in a toroid *Phys. Fluids* **1** 265
[35] Belli E A and Candy J 2018 Impact of centrifugal drifts on ion turbulent transport *Phys. Plasmas* **25** 032301
[36] Staebler G M, Waltz R E, Candy J and Kinsey J E 2013 A new paradigm for suppression of gyrokinetic turbulence by velocity shear *Phys. Rev. Lett.* **110** 055003
[37] Staebler G M, Kinsey J E and Waltz R E 2007 A theory-based transport model with comprehensive physics *Phys. Plasmas* **14** 055909
[38] McMillan B F, Joliet S, Tran T M, Villard L, Bottino A and Angelino P 2008 Long global gyrokinetic simulations: source terms and particle noise control *Phys. Plasmas* **15** 052308
[39] Belli E A and Candy J 2008 Kinetic calculation of neoclassical transport including self-consistent electron and impurity dynamics *Plasma Phys. Control. Fusion* **50** 095010
[40] Miller R L, Chu M S, Greene J M, Lin-liu Y R and Waltz R E 1998 Noncircular, finite aspect ratio, local equilibrium model *Phys. Plasmas* **5** 973
[41] Candy J, Holland C, Waltz R E, Fahey M R and Belli E 2009 Tokamak profile prediction using direct gyrokinetic and neoclassical simulation *Phys. Plasmas* **16** 060704
[42] Sugama H, Watanabe T-H and Nunami M 2009 Linearized model collision operators for multiple ion species plasmas and gyrokinetic entropy balance equations *Phys. Plasmas* **16** 112503
[43] Belli E A and Candy J 2015 Neoclassical transport in toroidal plasmas with nonaxisymmetric flux surfaces *Plasma Phys. Control. Fusion* **57** 054012